Anal. Method Environ. Chem. J. 3 (2) (2020) 92-107

AMECJ

Research Article, Issue 2
Analytical Methods in Environmental Chemistry Journal
Journal home page: www.amecj.com/ir

A new kinetic models analysis for CO adsorption on palladium zeolite nanostructure by roll-coating technique

Nastaran Mozaffari [a], Alireza Haji Seyed Mirzahosseini [a,*] and Niloofar Mozaffari [b]

[a] *Department of Environmental Engineering, Faculty of Natural Resources and Environment, Science and Research Branch, Islamic Azad University, Tehran, Iran*
[b] *Department of Physics, Faculty of Sciences, Science and Research Branch, Islamic Azad University, Tehran, Iran*

ARTICLE INFO:

Received 19 Feb 2020
Revised form 25 Apr 2020
Accepted 20 May 2020
Available online 30 Jun 2020

Keywords:
Carbon monoxide (CO),
Toxic gas analysis,
Adsorption,
Alumina palladium zeolite composite films,
Kinetic models

ABSTRACT

The aim of this article was the fabrication of *zeolite@Pd*/Al_2O_3 nanostructure through roll-coating technique for CO gas adsorption from air. Transmission electron microscopy (TEM), field-emission scanning electron microscopy (FESEM), X-ray diffraction (XRD), and energy-dispersive x-ray spectroscopy (EDX) were performed to investigate the morphological, structural, and elemental properties of *zeolite@Pd*/Al_2O_3 adsorbent. A continues carbon monoxide gas analyzer KIGAZ 210 was applied for analyzing of CO gas adsorption on as-present adsorbent in an experimental set-up. The adsorption capacity at equilibrium time for CO molecules was studied by *zeolite@Pd*/Al_2O_3 adsorbent. The Elovich, Avrami, and Fractional power kinetic models were used for this study. The equal value of experimental and theoretical adsorption capacity at equilibrium time as well as the unit value of regression coefficient was indicated that the Avrami kinetic model was the suitable model to describe CO removal from air through *zeolite@Pd*/Al_2O_3 nanostructure. The results showed us, the CO molecules were efficiently removed by catalytic zeolite adsorbent more than 95% from air at optimized conditions.

1. Introduction

The clean and high quality air is essential for human health. The main contributors to climate change belong to emission of toxic gases CO, CO_2, NO_x, So_x [1, 2]. Operations of industries and factories, transportation, agricultural activities and post/pre combustion of fuels are major reasons behind the emissions of CO and CO_2 in environment air. Carbon Monoxide (CO) as a main ecological pollutant, can be formed by incomplete burning of industrial fuels, automobiles and caused to a serious of symptoms including dizziness, naupathia and dyspnea [3, 4]. The acceptable limit of CO exposure has reported by ACGIH chemical substances [5]. The development of efficient and robust techniques for air purification has been boosting attention over the past few decades [6]. Among these techniques, the process of adsorption shows a fundamental surface phenomenon in which the attachment of solute (adsorbate) into a solid surface (adsorbent) can remove pollutants selectively from air atmosphere [6, 7]. According to the previous studies, some of toxic gases such as CO, CO_2, SO_2, O_3, VOC_s, etc., have more concentration in air [3]. Nowadays, excellent properties of nanomaterials such as high surface area and high adsorption

* Corresponding Author: Alireza Haji Seyed Mirzahosseini
Email: mirzahosseini@gmail.com
https://doi.org/10.24200/amecj.v3.i02.106

caused to use for air purification [8-10]. According to the most valence of equilibrium cycle, the cycle of adsorption/desorption process can be identified approximately when the adsorbent is started that the model of isotherm as fluctuation of temperature and or pressure can be applied for appraising of the maximum capacity of equilibrium axle. Moreover, the regeneration procedure can be estimated through adsorbents' recognizable characteristic like thermal behavior of electricity. Electric swing adsorption (ESA), moisture swing adsorption (MSA), temperature swing adsorption (TSA), and pressure swing adsorption (PSA), or techniques like temperature vacuum-pressure swing adsorption (TVPSA) that can be made by compilation of these above methods [11]. Pressure/Vacuum swing adsorption (PSA/VSA) and temperature swing adsorption (TSA) techniques was used for trapping of gas pollutions by above methods [12-15]. Carbon-based adsorbents such as activated carbons are commercially cheaper than other adsorbents, and also have known for toxic gas removal because of its useful properties such as eco-dependence, consistency of thermic and chemic, conductance of heat and electricity, or high resistance [16-19]. However, its disadvantages such as lack of low thermal and mechanical stability rather than other materials should not be ignored [6]. Recently, varieties of nonporous including metal-organic frameworks (MOFs) [20-23], mesoporous alumina (MA) [24, 25], and mesoporous silica (MS) [26,27] have been used for detection and adsorption of toxic gases, and are regarded as alternatives to commercial adsorbents [28,29]. Metal-organic frameworks (MOFs) are confirmed to be a significant adsorbent due to its unique properties such as large specific surface area, ultra-high porosities, controllable architectures, and low density [30, 31]. As an important factor, the porosity of MOFs can help to adsorb and desorbs micro molecules by providing a fast and handy path [32,33]. Although considerable fabricated and natural adsorbents such as activated carbon [26], fly ash [25], natural/modified clays [24], biomaterials [4], metal-organic-frameworks (MOFs) [23], zeolites [22,21], and nanomaterials [27] have been studied for a long period of time, there is still needs for advancements of adsorption technology and developing recyclable, cost-effective, high efficient adsorbents that have high capacity. Mesoporous alumina and other alumina-based substances have high adsorption capacity because of their interconnected channels, uniformed porous structures, and united pore size [34,35]. In particular, γ-Phase nano-Al_2O_3 is the best candidate for gas molecules capturing rather than other alumina phases known as "transition alumina" owing to its pore-volume, large surface area, and great catalytic activity [36, 37, 38]. The properties with high surface area and acidic surface make the gamma-alumina (γ-Al_2O_3) a unique material with extensive application ranging from adsorbents to heterogeneous catalysis [39-42]. The phases including δ-, η-, θ-, and γ - Al_2O_3 indicates one of various metastable stages (polymorphs) of alumina [39, 43, 44]. A higher CO adsorption and great capacity of adsorbents can be occurred by covering of the small particle size of Pd clusters on the Al_2O_3 surface [45]. The application of palladium is restricted due to its high material cost, even though there has been extensive investigation of nanopalladium or its alloy groups [46]. Therefore, in this study, nano-scale palladium II nitrate has used due to its similar unique and useful characteristics with palladium nanoparticles, and because of being cost-effective and easy to access compared to palladium. The mesoporous silicates are one of the promising kinds of nanoscale materials that become well-known for researchers due to their potential abilities and utilizations [47-53]. Several researchers have been reported the advantages of applying nanoscale zeolite (NPs) over micro-scale zeolite (MPs). [54-58] For example, according to results of comparing nano-scale (30-40 nm) and micro-scale (2000 nm) of H-ZSM-5 for its catalytic performance, it has found that the catalyst lifetime for H-ZSM-5 in nano-scale particles is longer than itself in micro-scale particles [58]. Synthesizing and utilizing nanosized zeolite attract great interests compared to zeolite with micron size, recently [54-62]. The properties of high external surface

area and high availability of active sites have been made nanoscale zeolites better catalytic proficiency and age of catalyst. Either a particular type of nanoadsorbents like CNTs [63,64], or some kinds of pollutants including heavy metal, antibiotic and so on [65, 66], or organic and inorganic pollutants removal [67] have totally been focused by most of recent review articles even though over 500 technical papers published between 2000 to 2019 indicate the rapid growth of interest in this research area. Hence, the current study concentrates on the adsorption of carbon monoxide as a toxic gas by nanomaterial based composite films. The present study's aim is firstly loading three nanoparticles γ-Al_2O_3, $Pd(NO_3)_2$ and zeolite on glass substrates through the roll-coating method, in order to enhance the span of reactions between CO gas molecules and adsorbents surface, and improve the ability of adsorbents for CO capturing. Then, the Elovich, the Avrami, and the Fractional power kinetic models for CO adsorption by zeolite@Pd/Al_2O_3 nanoadsorbent were studied and analyzed.

2. Experimental

2.1. Materials

Nanoshel chemicals was provided alumina nanoparticles (CASN: 1344-28-1, Molar mass: 101.96 g mol^{-1} γ-Al_2O_3 with purity >99.9%) and zeolite nanoparticles (CASN:1318-02-01, Al_2O_{34} SiO_2 H_2O with purity 99%). Merck chemicals and Sigma-Aldrich were two sources that 1-methyl-2-pyrrolidone and palladium nitrate ($Pd(NO_3)_2$) were bought from them, respectively. There were no needs for purification of received chemicals in order to use them.

2.2. Preparation of Adsorbent

The roll-coating technique has been used to deposit zeolite@Pd/Al_2O_3 as composite films on glass substrates. Four glass substrates (2 cm × 8 cm) were used in this study. Disinfectant materials such as acetone, ethanol and deionized water were consumed for washing glass substrates three times in an ultrasonic device. Then, the washed substrates dried at room temperature. As the process of samples preparation, firstly 1 g of Al_2O_3, 1 g of zeolite and 1 g of $Pd(NO_3)_2$ were mixed in a container, then 1-methyl-2-pyrrolidone was added dropwise into it as 10 mL in order to make the adhesion of materials on the substrates easy and stronger. After 1 day, the prepared coated substrates were desiccated at room temperature. Finally, a hollow cubic container was fabricated through attaching these four Al_2O_3/$Pd(NO_3)_2$/Zeolite coated substrates to each other whereby this tunnel-like shape helps CO gas molecules to be channeled and trapped readily [68]. In this case, the adsorption capacity and efficiency will be greatly affected by enhancing the rate of interaction between gas molecules and adsorbents.

2.3. Characterization

Transmission Electron Microscopy (TEM) was used in order to determine the shape and grain distribution of nanoparticles with high resolution. X-ray diffraction (XRD, STOE STADI MP) was applied for extracting the crystalline structure of pure initial materials. Topography and morphology of as-present adsorbent (before and after adsorption process) were determined through field emission scanning electron microscope (FESEM, MIRA3 TESCAN), while energy-dispersive X-ray spectroscopy (EDX) analysis was used in order to specify and measure chemical elemental contents of the sample.

2.4. Adsorption of CO

The schematic of designed experimental setup for testing CO adsorption consists of main three sections as a CO gas capsule, a compartment (20 cm length and 7 cm internal diameter) where an adsorbent is placed, and a carbon monoxide gas analyzer KIGAZ 210 (Sauermann Co, CO sensor protection by solenoid valve) based on tunable diode laser (TDL, LOD=1 ppm) for CO Measurement for detection of 1-120 ppm CO and evaluation of target gas (CO 99,999%) concentration [68]. The temperature of 0-250 °C (23-482 °F); optional (for probe installation) 0-600 °C (0-1112 °F) with additional thermal barrier was used. The constant pressure 1.5 bar was applied in this study. The

concentration of inlet CO gas and the saturation level of CO gas concentration were 150 mg L^{-1} and 5 mg L^{-1}, respectively.

2.5. Adsorption mechanism of CO by Zeolite@ Pd/Al_2O_3

Generally, movable and fixed bed are two types as classification of the adsorption/desorption by $Al_2O_3/Pd(NO_3)_2$/Zeolite. The molecules of gases like CO can attach to the adsorbent surface of $Al_2O_3/Pd(NO_3)_2$/Zeolite when the molecules of these gases achieve decreased free energy while the molecules come towards the surface of adsorbent. The value of CO molecules that come close to the surface of $Al_2O_3/Pd(NO_3)_2$/Zeolite adsorbent will be increased by decreasing of entropy that occurs by interplay between solid surface and CO molecules. The adsorption process based on van der Waals forces called physically adsorption, while chemical bond formation obtained between surface of $Al_2O_3/Pd(NO_3)_2$/Zeolite adsorbent and adsorbate. So, there are different mechanisms of physio-chemisorption for adsorption procedure which must be optimized. The MOFs' surface has several functional groups caused to act chemical reaction in mechanism adsorption [16]. In Order to achieve efficient elimination of CO, the adsorbent substance should possess some essential properties which are demonstrated as follow: 1) Since the proficiency of adsorption can specify how many adsorbents are required whereby the adsorption column's volume can be measured, it possesses high importance for determining the main cost of the adsorption mechanism. However, the value of adsorbent and size of equipment for adsorption process must be minimized due to high CO concentration. 2) The ratio of CO to another gas capacity shows the selectivity CO gas. 3) Another parameter for grading the adsorbents' efficiency is the kinetics of adsorption/desorption that the fast rate of adsorption/desorption kinetics for CO will be required by the adsorbents. The cycle of time will be controlled by processes of regeneration and the adsorption's kinetics that can form two types of curves that are a sharp breakthrough curve for CO which indicates a fast kinetics, and a budged breakthrough curve occurs if there is slow kinetics for CO. The transfer of mass through the surface of adsorbent, the functional group on the surface of adsorbent, and carbon monoxide's reaction kinetics can together influence on the kinetics of CO adsorption on the porous substances. 4) In order to keep high kinetics, it is necessary to have a property of the mechanical stability for adsorbent. 5) The demanded energy for regeneration of adsorbents should be measured. The range of -25 to -50 kJ mol^{-1} is allocated to heat of physisorption and chemisorption cases possess the heat of -60 to -90 kJ mol^{-1} [17]. Regarding the chemical adsorbents, physical adsorbents such as carbonaceous and non-carbonaceous substances need low energy desire for CO removal due to the no generation of new bonds between these gases and the adsorbents' surface whereby the regeneration of these gases requires less energy (Fig.1).

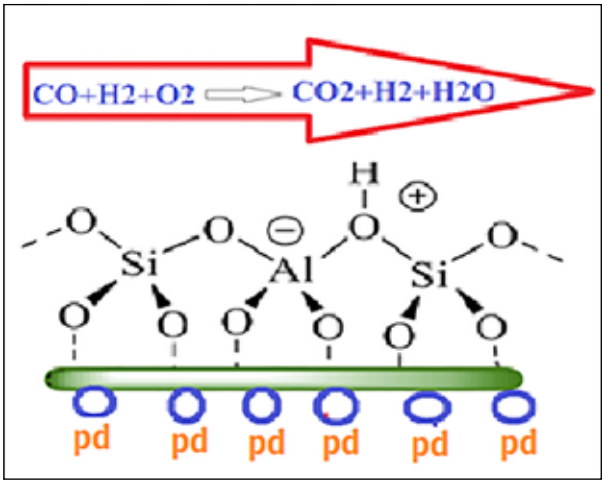

Fig.1. The adsorption mechanism of CO by zeolite@ Pd/Al_2O_3 adsorbent

3. Results and discussion

3.1. TEM analysis

Figure 2a demonstrates the results of TEM analysis of pure Al_2O_3 nanoparticles (γ-Al_2O_3) that three dimensional porous structure are made up by interconnected rod-like particles [69]. It is obviously shown that the shape of nanoparticles does not look accurately spherical [70]. The TEM for nanoparticles of zeolite and zeolite@Pd/Al_2O_3 was shown in Figure 2b and 2C, respectively.

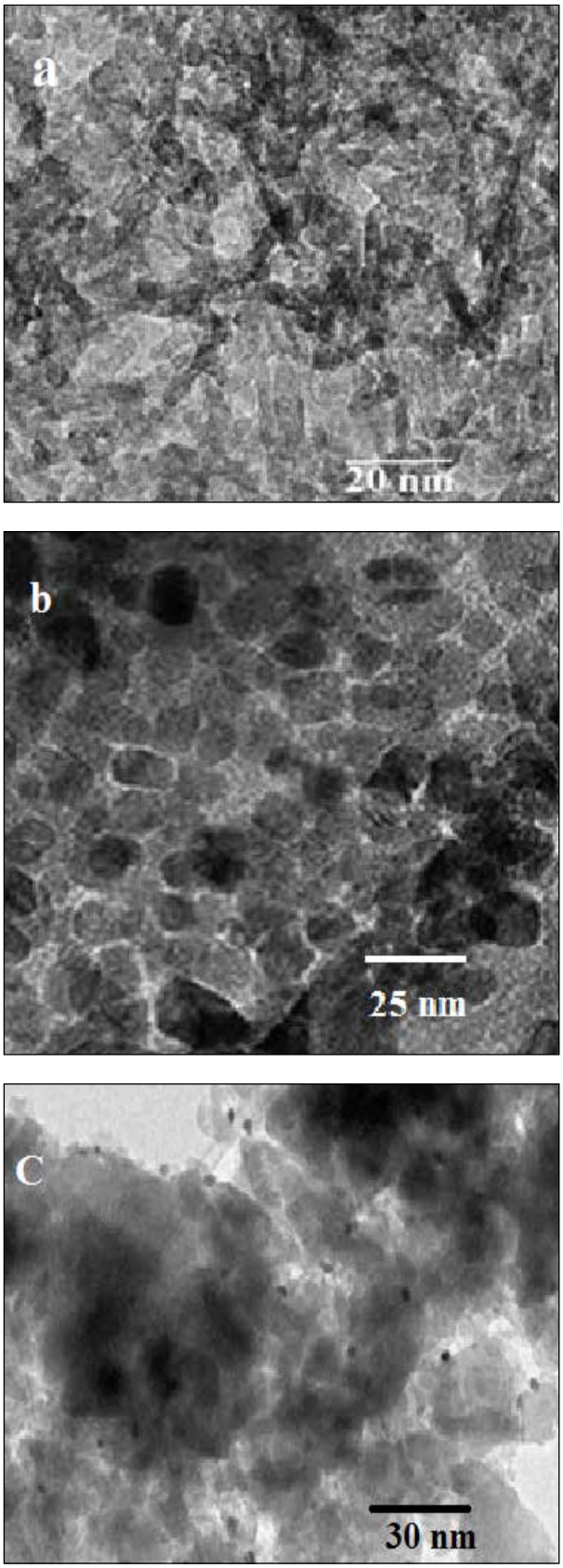

Fig. 2. The TEM for different nanoparticles **a)** γ-Al_2O_3 **b)** Zeolite **c)** Zeolite@Pd/Al_2O_3

3.2. XRD spectra

Figure 3 shows the XRD patterns of pure initial materials which are Al_2O_3, $Pd(NO_3)_2$ and zeolite. An X-ray diffractometer with Cu Kα source (λ = 1.5405 Å) and a scan step size of 0.01° was used for recording XRD patterns. The range of scanning (2θ) was recorded between 10° and 90°. As it is shown, the structure of pure zeolite nanoparticles is more crystalline than pure Al_2O_3 and $Pd(NO_3)_2$ nanoparticles that confirm an appropriate property of zeolite to have a high adsorption capacity due to its porosity. The diffraction peaks of the pure Al_2O_3 appeared at 2θ of 31.93°, 39.49°, 45.49° and 66.76° which are well distributed to the crystalline preferred orientation of 220, 222, 400 and 440, respectively. The peak positions of $Pd(NO_3)_2$ were considered as 24.079 and 68.08, which are corresponding to 011 and 220, respectively. The diffraction peaks 10.34, 16.56, 21.79, 29.39 and 31.58, corresponding to the reflection from 220, 212, 203, 451 and 002 are observed in zeolite nanoparticles. The characteristic peaks of pure zeolite are well matched and consistent with the corresponding peaks of all samples, and there are no other observed phases. [71] According to XRD patterns of pure zeolite, there is no considerable alteration in the framework and no lost in solid pure zeolite's crystallinity as well as the host frame stays intact at the end of the mechanism. [72] Al_2O_3 nanoparticles (Ref 00-029-0063), $Pd(NO_3)_2$ (Ref 00-005-0681 and 01-087-0643) and zeolite (Ref 01-080-0922) are in good agreement with the candidate references (Table 1). Regarding the fact that available commercial nanomaterials of γ-Al_2O_3 produced through boehmite thermal dehydration, thus determining the crystal structure of γ-Al_2O_3 is difficult as well as it indicates poor crystallinity and impurities. Also, this fact can include other alumina polymorphs that have similar crystal formations. The appropriate structure for analysis belongs to large, clean γ-Al_2O_3 single-crystals that typically cannot produced commercially. Oxidizing single-crystal NiAl (110) under appropriate-controlled conditions would make single-crystal γ-Al_2O_3 films with more than 80 nm thick able to be grown

Table 1. The obtained crystalline regions and peaks of the zeolite@Pd/Al_2O_3 composite film ($Al_2O_3/Pd(NO_3)_2$/zeolite) through XRD patterns[73]

Al_2O_3	**hkl**	**220**	**222**	**400**	**440**	
	2θ (Degree)	31.93°	39.49°	45.49°	66.76°	
$Pd(NO_3)_2$ 2 (Degree)	**hkl**	**011**	**-----**	**-----**	**220**	
	2θ (Degree)	24.079°	-----	-----	68.08°	
Zeolite 2 (Degree)	**hkl**	**220**	**212**	**203**	**451**	**002**
	2θ (Degree)	10.34°	16.56°	21.79°	29.39°	31.58°

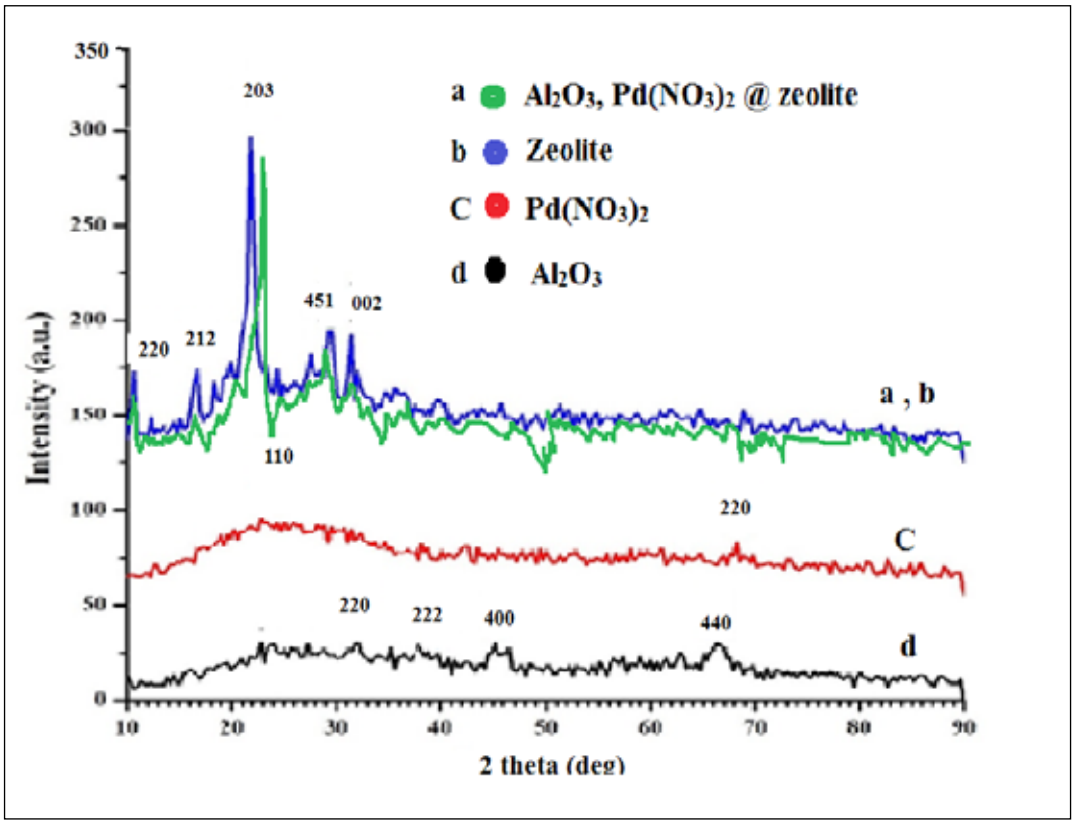

Fig. 3. The results of XRD analysis for pure initial materials including a) $Al_2O_3/Pd(NO_3)_2$/zeolite b) zeolite, c) $Pd(NO_3)_2$ and d) Al_2O_3 nanoparticles

which is demonstrated by Zhang et al which were worked on Al_2O_3 with γ-shape structure on Ni-Al. Since γ-Al_2O_3 fabricated by this technique is well crystalline and does not possess hydrogen or water in bulk structure, it is suitable for considered structural analysis, unlike the material boehmite-originated γ-Al_2O_3 [73].

3.3. FESEM spectra

The surface morphology, microstructure, particle size and distribution of the as-prepared product are determined by field emission scanning electron microscope (FESEM). Figure 4 indicates the FESEM images of the $Al_2O_3/Pd(NO_3)_2$/Zeolite sample at a 1 μm scale of magnification before

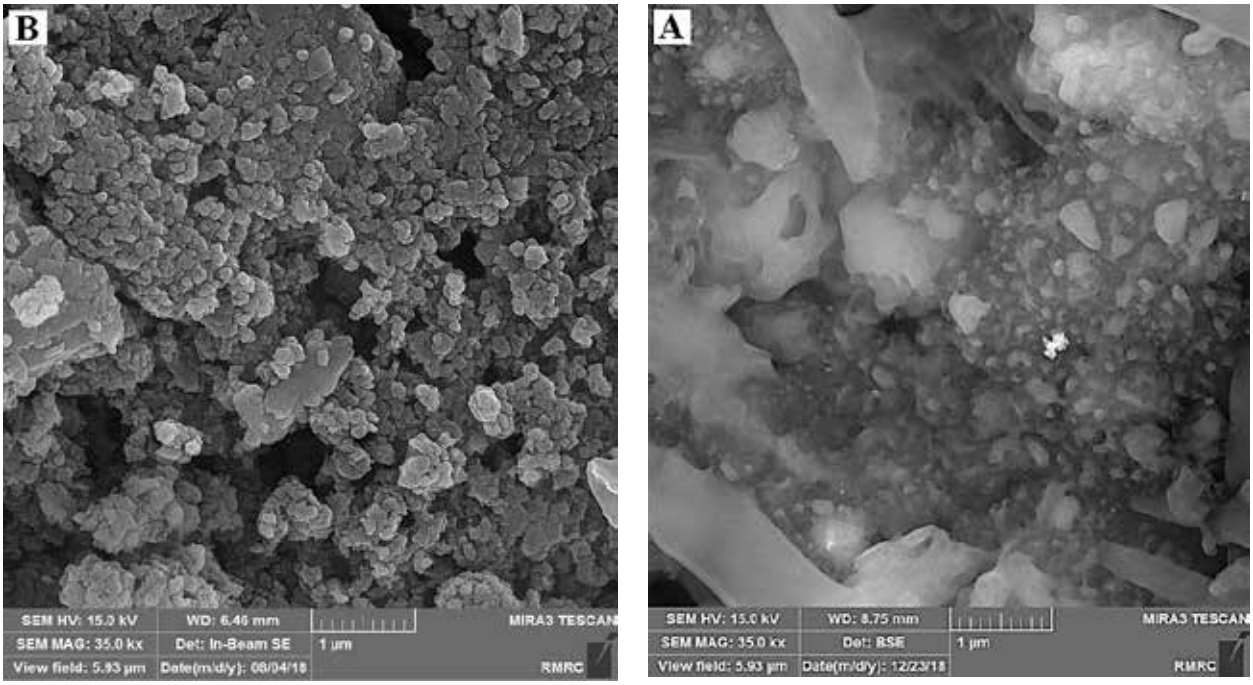

Fig. 4. Obtained images from FESEM of $Al_2O_3/Pd(NO_3)_2$/zeolite adsorbent a) Before b) after CO gas adsorption at 1 µm scales of magnification.

and after CO gas adsorption. The FESEM results revealed that the united porous structures along with regular interlinked channels are developed throughout the adsorbents after adsorption. Also, homogenous dispersion and well particle size repartition of adsorbent after the adsorption process make it incomparable than its virgin version. Hence, a high surface area and whereby a very high CO adsorption is noticed because of these properties.

3.4. Energy-dispersive X-ray spectroscopy

The percentage of elemental content was determined by energy-dispersive X-ray spectroscopy (EDX). Figure 5 illustrates the existence of Al, O, Si, Pd, and N in the sample before the adsorption process that was utilized to fabricate as-present adsorbent. Since Al_2O_3 and zeolite (aluminum silicates) nanoparticles were used in this study, a notable increase in the spectral position of Al EDX peak is observed. The weight and atomic percentages of ingredients are extracted from EDX patterns of virgin adsorbent that include Al, O, Pd, N, and Si at wt.% for each element. (Table 2) The peak of Ca corresponds to glass substrates.

3.5. Kinetic models analysis

The inlet CO gas concentration into an experimental set-up considered as 150 mg L^{-1}. The evaluation of various concentrations of adsorbed CO versus time for $Al_2O_3/Pd(NO_3)_2$/Zeolite adsorbent's results indicates the increase of adsorbed CO concentration (mg L^{-1}) with passing time until reaching saturation levels [68]. The relation between adsorbed CO gas concentration and contact time was illustrated in Figure 6. This diagram indicated the effect of passing time on the speed of CO adsorption that becomes slower while time is reaching saturation level. As it is obvious, the adsorbed CO gas concentration is decreased as range of 150-70, 69-11 and 10-5 mg L^{-1} at rate of 1 s, 2 s and 3 s, respectively.

Table 2. Statistical analysis EDX results of $Al_2O_3/Pd(NO_3)_2$/zeolite with its atomic and weight values.

Elements	Al K_a	O K_a	Pd K_a	N K_a	Si K_a	Ca K_a
wt.%	8.21	26.46	45.01	0.53	1.62	0.48
at%	7.78	42.33	10.83	0.59	1.47	0.31

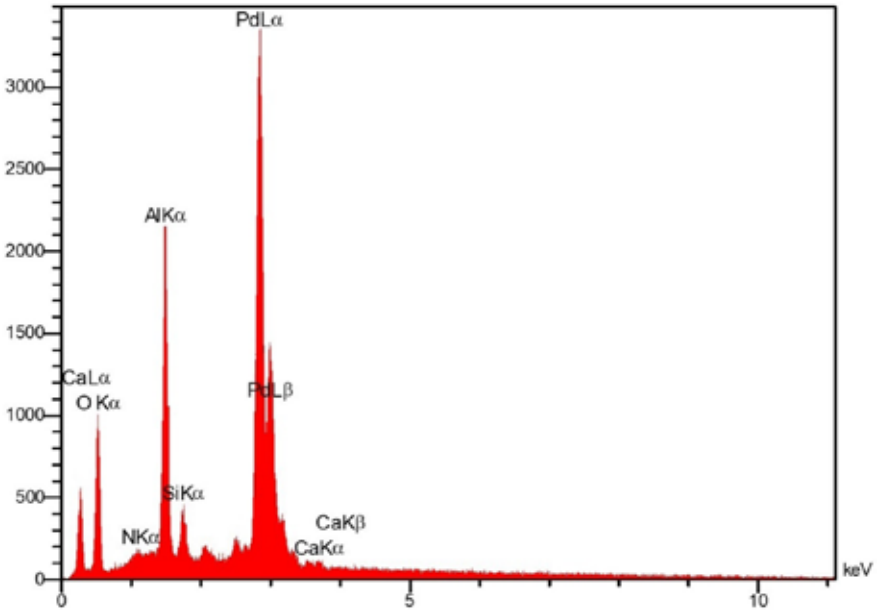

Fig. 5. EDX patterns of the made $Al_2O_3/Pd(NO_3)_2$/zeolite adsorbent

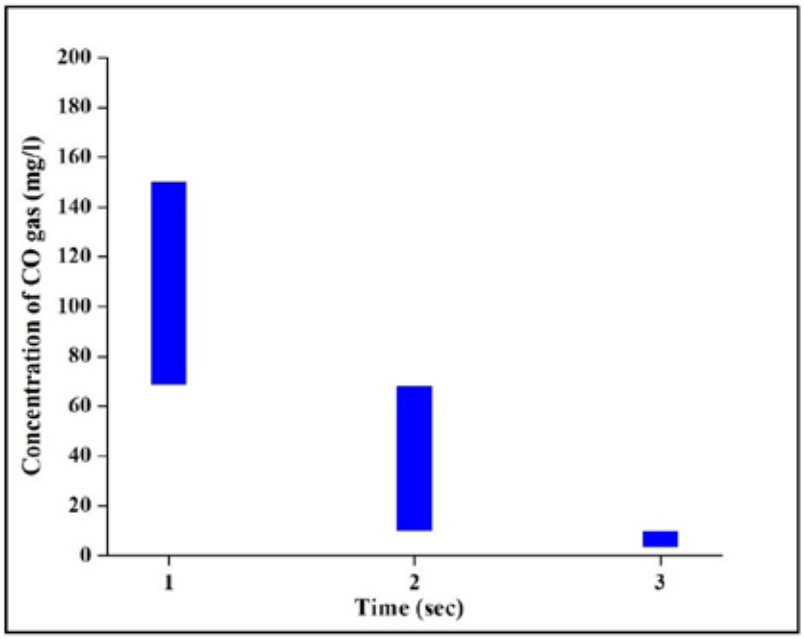

Fig. 6. The diagram of relation between adsorbed CO gas concentration and contact time (mg L^{-1}, sec)

To explore the chemisorption kinetic of gases onto a solid surface, Elovich kinetic model is describe [74, 75]. The Elovich kinetic introduced in Equation 1 [76].

$$q_t = \frac{1}{\beta} Ln(\alpha\beta) + \frac{1}{\beta} \mathrm{Ln}\, t \qquad \text{(Eq. 1)}$$

Where q_t is adsorption capacity at time t (mg g^{-1}), the Elovich coefficient α in the primary rate of adsorption (mg g^{-1} min^{-1}), and the Elovich coefficient β is desorption rate constant (g mg^{-1}) that is associated to the extent of energy activation as well as surface covering for chemisorption process.

The amount of α and β are obtained from intercept (β^{-1} Ln(αβ)) and slope (β^{-1}) of q_t vs. Ln t linear plot (Fig. 7). It should be noted that the number of remained sites after adsorption process can be specified by the value of β^{-1}, and adsorption quantity in Ln t = 0. It can be shown by β^{-1} Ln(αβ) value that the closeness of this value with experimental value indicates the best fitting of kinetic data to the Elovich model [77], however, in this research work, the values have significant difference. The obtained parameters were listed in Table 3. Regarding Mozaffari et al. 2020 [68], the amount of experimental equilibrium adsorption capacity at 216 s is 111.16 mg. g^{-1} that is not in agreement with the theoretical adsorption capacity at equilibrium time calculated through this model. The low regression coefficient (R^2) value and unequal value of $q_{e.exp}$ as well as $q_{e.cal}$ demonstrate the scantiness Elovich model of for description of CO removal by Al_2O_3/$Pd(NO_3)_2$/Zeolite nano-adsorbent.

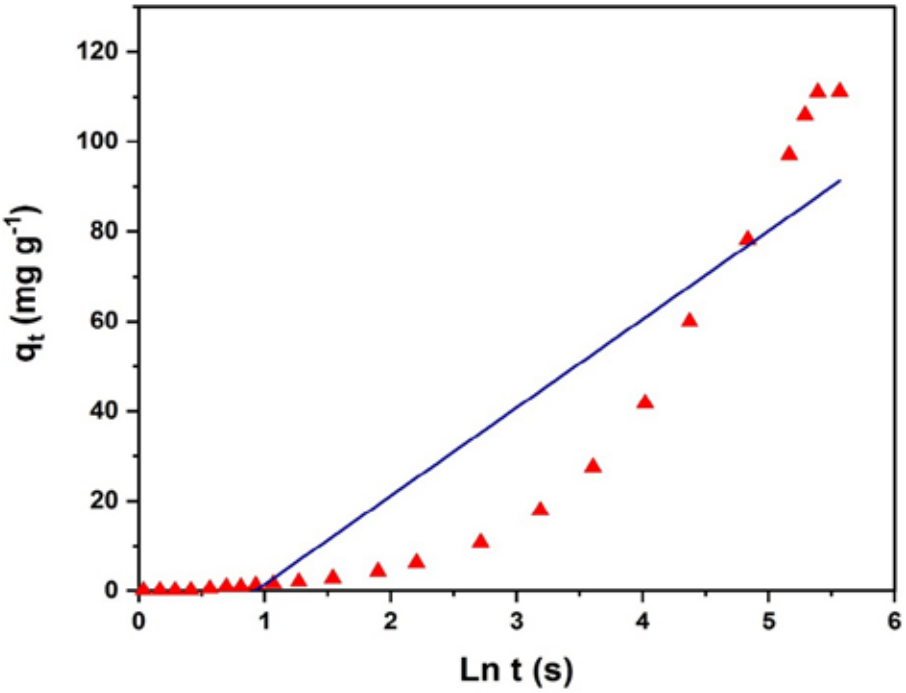

Fig. 7. The Elovich kinetic model for carbon monoxide adsorption by Al_2O_3/$Pd(NO_3)_2$/Zeolite nano-adsorbent

Table 3. The calculated parameters of the Elovich, Avrami, and Fractional power kinetic models

$q_{e,exp}$ (mg.g^{-1})		111.16		[99]	
Elovich Model		**Avrami Model**		**Fractional Power Model**	
$q_{e,cal}$	91.94	$q_{e,cal}$	111.16	$q_{e,cal}$	129.93
α	٣,٥	k_{AV}	4.54	k	1.048
β	٠,٠٣٦	n_{AV}	1.12	v	0.896
β^{-1}	28.096	R^2	0.99	R^2	0.98
β^{-1} [Ln(αβ)]	58.29				
R^2	0.85				

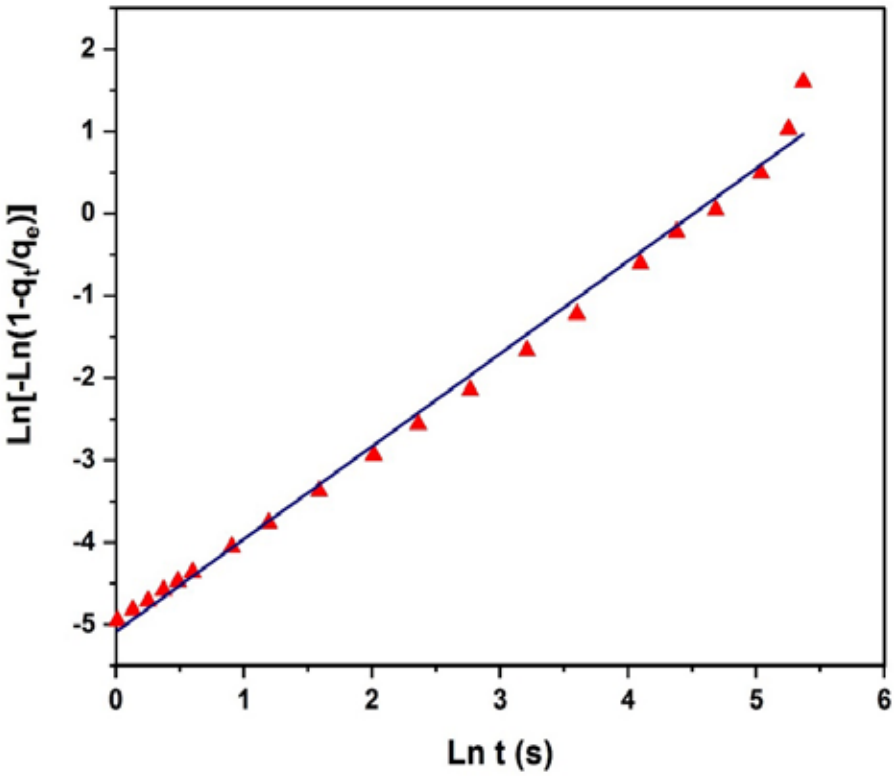

Fig. 8. The Avrami kinetic model for carbon monoxide adsorption by Al_2O_3/$Pd(NO_3)_2$/Zeolite nano-adsorbent

For simulation of phase transition as well as the growth of crystallite in adsorbent, Avrami kinetic model is investigated [78]. The Avrami kinetic is expressed in equation 2 [79]:

$$Ln\left[Ln\left(1-\frac{q_t}{q_e}\right)\right] = n_{AV}k_{AV} + n_{AV}Ln\ t \quad \textbf{(Eq. 2)}$$

Where K_{AV} is the Avrami kinetic constant, the n_{AV} is the Avrami exponent to hypothesize the mechanism of alteration during the process of adsorption [109]. The amount of K_{AV} and n_{AV} are acquired from intercept and slope of $Ln[-Ln\left(1-\frac{q_t}{q_e}\right)]$ vs. Ln linear plot.

Figure 8 demonstrates the plot of $Ln[-Ln\left(1-\frac{q_t}{q_e}\right)]$ versus. The regression coefficient (R^2) is close to unity that shows the best fit of data. The value of theoretical adsorption capacity at (equilibrium time) was obtained as 111.16 mg g^{-1} that is match with the experimental equilibrium adsorption capacity which was reported by Mozaffari et al 2020 [68]. Table 3 gives the calculated parameters of this model. Therefore, the unit value of R^2 and identical value of and indicate the best applicability of Avrami kinetic model to describe carbon monoxide adsorption through $Al_2O_3/Pd(NO_3)_2$/Zeolite nano-adsorbent.

The modified form of the Freundlich equation is Fractional power model [80]. Fractional power kinetic model is defined as equation 3 [110].

$$Lnq_t = Ln\ k + vLn\ t \quad \textbf{(Eq. 3)}$$

Where k and v are constants and v should be less than unity. The sorption rate at is defined as kv [80]. The plot of versus is demonstrated in Figure 9. The amount of k and v are obtained from intercept (Ln k) and slope (v) of vs. linearplot.

The calculated constants are tabulated in Table 3. The value of v was obtained as 0.89 that is positive and less than unity and regression coefficient (R^2)

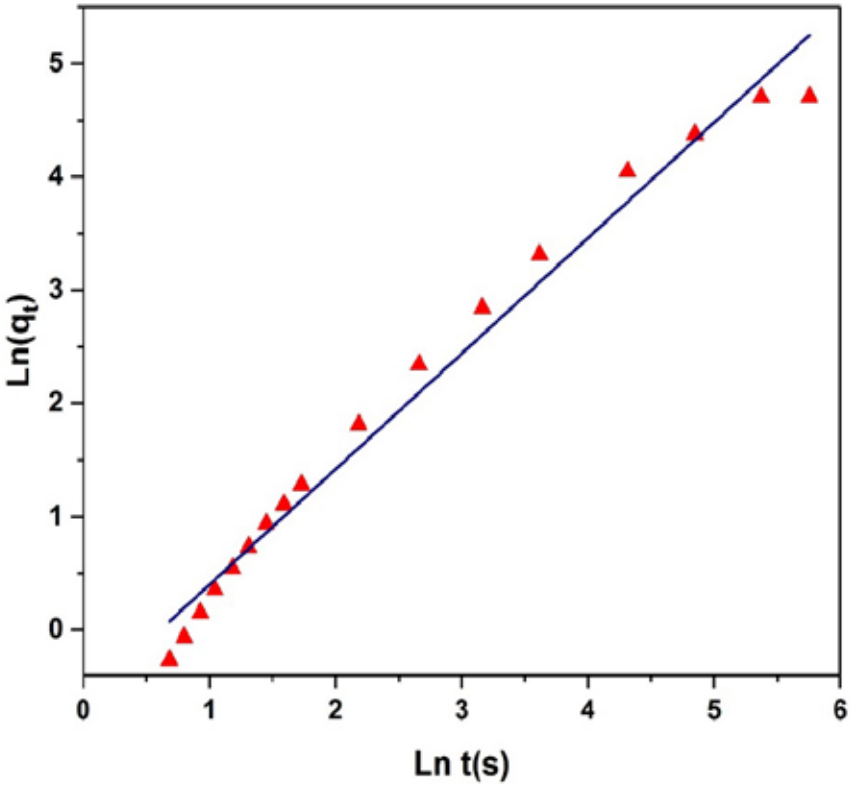

Fig. 9. The Fractional power kinetic model for carbon monoxide adsorption by $Al_2O_3/Pd(NO_3)_2$/Zeolite nano-adsorbent

is almost close to unity. However, experimental adsorption capacity at equilibrium time that was obtained by [99] is not in a good agreement with calculated adsorption capacity. Thus, this model is not sufficient to describe carbon monoxide by $Al_2O_3/Pd(NO_3)_2$/Zeolite nano-adsorbent.

4. Conclusions

In this article, $Al_2O_3/Pd(NO_3)_2$/zeolite adsorbent was prepared by roll coating method to investigate its ability to remove CO gas. It was shown that the effect of passing time on the speed of CO adsorption that becomes slower while time is reaching saturation level. To study the kinetic models for CO removal through this adsorbent, the Elovich, Avrami, and Fractional power kinetic models were explored. The investigation of Avrami kinetic model illustrated that the experimental and theoretical adsorption capacity value at equilibrium time was identical. Furthermore, the regression coefficient value (R^2) was close to unity. Therefore, the Avrami kinetic model was the best model to describe CO removal through $Al_2O_3/Pd(NO_3)_2$/zeolite adsorbent. The porous structure of $Al_2O_3/Pd(NO_3)_2$/zeolite adsorbent which was obtained from FESEM analysis is responsible for high values of adsorption efficiency and adsorption capacity. The result of XRD patterns of pure initial materials was applied to confirm their purity and crystalline structures. Elemental content of materials of adsorbent before adsorption was specified by EDX analysis to show the existence of Al, O, Pd, Si, N and Ca that the last one was referred to glass substrates.

5. Acknowledgement

This study was carried out in Natural Recourses College Lab, Environment Science and Research Department.

6. References

[1] J. Cleland, World population growth; past, present and future, Environ. Res. Econ., 55 (2013) 543–554.

[2] M. Hussain, G. Liu, B. Yousaf, R. Ahmed, F. Uzma, M. U. Ali, H. Ullah, A. R. Butt, Regional and sectoral assessment on climate-change in Pakistan: Social norms and indigenous perceptions on climate-change adaptation and mitigation in relation to global context, J. Clean. Prod., 200 (2018) 791–808.

[3] S, Mahajan. S, Jagtap, Metal-oxide semiconductors for carbon monoxide (CO) gas sensing. Materials. Rev., 18 (2020) 100483.

[4] C. Qin, B. Wang, N. Wu, C. Han, C. Wu, X. Zhang, Q. Tian, S. Shen, P. Li, Y. Wang, Metal-organic frameworks derived porous Co_3O_4 dodecahedrons with abundant active Co^{3+} for ppb-level CO gas sensing, Appl. Surf. Sci., 506 (2019) 144900.

[5] ACGIH Chemical Substances TLV Committee, Notice of intended change - carbon monoxide, Appl. Occup. Environ. Hyg., 6 (1991) 621–624.

[6] A. M. Awad, R. Jalab, A. Benamor, M. S. Naser, M. M. Ba-Abbad, M. El-Naas, A. W. Mohammad, Adsorption of organic pollutants by nanomaterial-based adsorbents: An overview. J. Mol. Liq., 301 (2019) 112-335.

[7] M. N. Rashed, Adsorption technique for the removal of organic pollutants from water and wastewater, Organic Pollutants-Monitoring, Risk and Treatment, Intech. Open, (2013) 167-194.

[8] P. K. Gautam, A. Singh, K. Misra, A. K. Sahoo, S. K. Samanta, Synthesis and applications of biogenic nanomaterials in drinking and wastewater treatment, J. Environ. Manage., 231 (2019) 734–748.

[9] C. Santhosh, V. Velmurugan, G. Jacob, S. K. Jeong, A. N. Grace, A. Bhatnagar, Role of nanomaterials in water treatment applications: A review, Chem. Eng. J., 306 (2016) 1116– 1137.

[10] Y. Zhang, B. Wu, H. Xu, H. Liu, M. Wang, Y. He, B. Pan, Nanomaterials-enabled water and wastewater treatment, Nano Impact, 3 (2016) 22–39.

[11] R. Zhao, S. Deng, S. Wang, L. Zhao, Y. Zhang, B. Liu, H. Li, Z. Yu, Thermodynamic research of adsorbent materials on energy efficiency of vacuum pressure swing adsorption cycle for CO capture, Appl. Thermal Eng., 128 (2018) 818–829.

[12] K. T. Chue, J. N. Kim, Y. J. Yoo, S. H. Cho, R. T. Yang, Comparison of activated carbon and zeolite 13X for CO_2 recovery from flue gas by pressure swing adsorption, Ind. Eng. Chem. Res., 2 (1995) 591– 598.

[13] R, Krishna, Adsorptive separation of CO_2/CH_4/CO gas mixtures at high pressures, Micropor. Mesopor. Mater., 156 (2012) 217–223.

[14] M. Clausse, J. Bonjour, F. Meunier, Adsorption of gas mixtures in TSA adsorbers under various heat removal conditions, Chem. Eng. Sci., 17 (2004) 3657–3670.

[15] J.-R. Li, R. J. Kuppler, H. C. Zhou, Selective gas adsorption and separation in metal–organic frameworks, Chem. Soc. Rev., 5 (2009) 1477.

[16] M., Bui, C. S. Adjiman, A. Bardow, E. J. Anthony, A. Boston, S. Brown, et. Al., Carbon capture and storage (CCS): the way forward, Energ. Environ. Sci., 5 (2018) 1062–1176.

[17] A. Samanta, A. Zhao, G. K. H. Shimizu, P. Sarkar, R. Gupta, Post combustion CO_2 capture using solid sorbents: a review, Ind. Eng. Chem. Res., 4 (2011) 1438–1463.

[18] D. Lozano-Castelló, D. Cazorla-Amorós, A. Linares-Solano, D. F. Quinn, Activated carbon monoliths for methane storage: influence of binder, Carbon, 15 (2002) 2817–2825.

[19] P. Bilalis, D. Katsigiannopoulos, A. Avgeropoulos, G. Sakellariou,

Noncovalent functionalization of carbon nanotubes with polymers, RSC Adv., 6 (2014) 2911– 2934.
[20] Y. K. Mishra, R. Adelung, ZnO tetrapod materials for functional applications, Mater. Today, 21 (2018) 631-651.
[21] X. Wang, W. Tian, T. Zhai, C. Zhi, Y. Bando, D. Golberg, Cobalt (II, III) oxide hollow structures: fabrication, properties and applications, J. Mater. Chem., 22 (2012) 23310-23326.
[22] N. S. Bobbitt, M. L. Mendonca, A. J. Howarth, T. Islamoglu, J. T. Hupp, O. K. Farha, R. Q. Snurr, Metal–organic frameworks for the removal of toxic industrial chemicals and chemical warfare agents, Chem. Soc. Rev., 46 (2017) 3357-3385.
[23] D. Britt, D. Tranche Montagne, O. M. Yaghi, Metal–organic frameworks with high capacity and selectivity for harmful gases, Proc. Natl. Acad. Sci., 105 (2008) 11623–1162.
[24] S. E. Lehman, S. C. Larsen, Zeolite and mesoporous silica nanomaterials: greener syntheses, environmental applications and biological toxicity, Environ. Sci. Nano, 1 (2014) 200-213.
[25] N. Moitra, P. Trens, L. Raehm, J.O. Durand, X. Cattoen, M. Wong Chi Man, Facile route to functionalized mesoporous silica nanoparticles by click chemistry, J. Mater. Chem., 21 (2011) 13476-13482.
[26] C. Yeom, Y. Kim, Mesoporous alumina with high capacity for carbon monoxide adsorption, Korean J. Chem. Eng., 35 (2017) 587–593.
[27] A. Walcarius, L. Mercier, Mesoporous organosilicon adsorbents: Nano engineered materials for removal of organic and inorganic pollutants, J. Mater. Chem., 20 (2010) 4478–4511.
[28] C. Yeom, R. Selvaraj, Y. Kim, Preparation of nonporous alumina using aluminum chloride via precipitation templating method for CO adsorbent, J. Ind. Eng. Chem., 67 (2017) 132-139.
[29] Z. Li, J.C. Barnes, A. Bosoy, J.F. Stoddart, J.I. Zink, Mesoporous silica nanoparticles in biomedical applications, Chem. Soc. Rev., 41 (2012) 2590–2605.
[30] T. Kitao, Y. Zhang, S. Kitagawa, B. Wang, T. Uemura, Hybridization of MOFs and polymers, Chem. Soc. Rev., 46 (2017) 3097–348.
[31] X. Lian, Y. Fang, E. Joseph, Q. Wang, J. Li, S. Banerjee, C. Lollar, X. Wang, H. Zhou, Enzyme-MOF (metal-organic framework) composites, Chem. Soc. Rev., 46 (2017) 3386-3401.
[32] L. Peng, J. Peng, Z. Xue, B. Han, J. Li, G. Yang, Large-pore mesoporous Mn_3O_4 crystals derived from metal-organic frameworks, Chem. Commun., 49 (2013) 11695-11697.
[33] R. K. Bhakta, J. L. Herberg, B. Jacobs, A. Highley, R. B. Jr, N. W. Ockwig, J. A. Greathouse, M. Alendorf, Metal-organic frameworks as templates for nanoscale NaAlH4, J. Am. Chem. Soc., 131 (2009) 13198–13199.
[34] S. Rengaraj, Y. Kim, J-W. Yeon, W-H. Kim, Application of Mg-mesoporous alumina prepared by using magnesium stearate as a template for the removal of nickel: kinetics, isotherm, and error analysis, Ind. Eng. Chem. Res., 46 (2007) 2834-2842.
[35] L. Dejam, S. Solaymani, A. Achour, S. Stach, S. Talu, N. Beryani Nezafat, V. Dalouji, A.A. Shokri, A. Ghaderi, Correlation between surface topography, optical band gaps and crystalline properties of engineered AZO and CAZO thin films, Chem. Phys. Lett., 719 (2019) 78-90.
[36] P. Souza Santos, H. Souza Santos, S.P. Toledo, Standard transition alumina. Electron microscopy studies, Mat. Res., 3 (2000) 104-114.

[37] M. Macêdo, C. Bertran, C. Osawa, Kinetics of the γ → α -alumina phase transformation by quantitative X-ray diffraction, J. Mater. Sci., 42 (2007) 2830–2836.

[38] C.H., Shek, J.K.L. Lai, T.S. Gu, G.M. Lin, Transformation evolution and infrared absorption spectra of amorphous and crystalline nano-Al_2O_3 powders, Nanostruct. Mater., 8 (1997) 605-610.

[39] J.L. Peng, L.D. Lai, X. Jiang, W.J. Jiang, B. Lai, Catalytic ozonation of succinic acid in aqueous solution using the catalyst of Ni/Al_2O_3 prepared by electroless plating-calcination method, Sep. Purif. Technol,. 195(2018) 138–148.

[40] N. Mozaffari, N. Mozaffari, S. M. Elahi, S. Vambol, V. Vambol, N. A. Khan, N. Khan, Kinetics study of CO molecules adsorption on Al_2O_3/Zeolite composite films prepared by roll-coating method, Surface Engineering. (2020) 1-10. https://doi.org/10.1080/02670844.2020.1768628

[41] M. Trueba, S.P. Trasatti, γ-Alumina as a support for catalysts: a review of fundamental aspects, Eur. J. Inorg. Chem., 17 (2005) 3393-3403.

[42] G. Busca, The surface of transitional aluminas: a critical review, Catal. Today, 226 (2014) 2-13.

[43] I. Levin, D. Brandon, Metastable alumina polymorphs: crystal structure and transition sequences, J. Am. Ceramic Soc., 81 (1998) 1995-2012.

[44] N. Mozaffari, S. Solaymani, A. Achour, S. Kulesza, M. Bramowicz, N. B. Nezafat, Ş. Ţălu, N. Mozaffari, S. Rezaee, New insights into SnO_2/Al_2O_3, Ni/Al_2O_3, and $SnO_2/Ni/Al_2O_3$compositefilms for CO adsorption: building a bridge between microstructures and adsorption properties, J. Phys. Chem. C, 124 (2020) 3692–3701.

[45] I. W. Davies, L. Matty, D. L. Hughes and P. J. Reider, Are heterogeneous catalysts precursors to homogeneous catalysts, Chem. Soc., 123 (2001) 10139-10140.

[46] I. Saldan, Y. Semenyuk, I. Marchuk, O. Reshetnyak, Chemical synthesis and application of palladium nanoparticles, J. Mater. Sci., 50 (2015) 2337-2354.

[47] N. Ono, The Nitro Group in Organic Synthesis; Wiley-VCH: Weinheim, 392, (2001). https:/doi: 10.1021/op010046s.

[48] G. Yan, M. Yang, Recent advances in the synthesis of aromatic nitro compounds. Org. Biomol. Chem., 11 (2013) 2554-2566.

[49] P. LaBeaume, M. Placzek, M. Daniels, I. Kendrick, P. Ng, M. McNeel, R. Afroze, A. Alexander, R. Thomas, A. E. Kallmerten, G. B. Jones, Microwave-accelerated fluorodenitrations and nitrodehalogenations: expeditious routes to labeled PET ligands and fluoropharmaceuticals, Tetrahedron Lett., 51 (2010) 1906-1909.

[50] X.-F. Wu, J. Schranck, H. Neumann, M. Beller, Convenient and mild synthesis of nitroarenes by metal-free nitration of arylboronic acids, Chem. Commun., 47 (2011) 12462-12463.

[51] J. P. Das, P. Sinha, S. Roy, A Nitro-Hunsdiecker Reaction: From Unsaturated Carboxylic Acids to Nitrostyrenes and Nitroarenes, Org. Lett., 4 (2002) 3055-3058.

[52] J. J. Song, J. T. Reeves, F. Gallou, Z. Tan, N. K. Yee, C. H Senanayake, Organometallic methods for the synthesis and functionalization of azaindoles, Chem. Soc. Rev., 36 (2007) 1120-1132.

[53] S. Mohan, P. Dinesha, S. Kumar, NOx reduction behaviour in copper zeolite catalysts for ammonia SCR systems: A review, Chem. Eng. J., 384 (2019) 123253.

[54] L. Tosheva, V.P. Valtchev, Nanozeolites: synthesis, crystallization mechanism, and applications, Chem. Mater., 17 (2005) 2494-2513.

[55] G. T. Vuong, V. T. Hoang, D. T. Nguyen, T. O. Do, Synthesis of nanozeolites and nanozeolite-based FCC catalysts, and their catalytic activity in gas oil cracking reaction, Appl. Catal. A, 382 (2010) 231-239.

[56] H. Konno, T. Okamura, T. Kawahara, Y. Nakasaka, T. Tago, T. Masuda, Kinetics of n-hexane cracking over ZSM-5 zeolites – Effect of crystal size on effectiveness factor and catalyst lifetime, Chem. Eng. J., 207–208 (2012) 490-496.

[57] T. Tago, H. Konno, Y. Nakasaka, T. Masuda, Size-controlled synthesis of nano-zeolites and their application to light olefin synthesis, Catal. Surv. Asia, 16 (2012) 148-163.

[58] T. Tago, H. Konno, M. Sakamoto, Y. Nakasaka, T. Masuda, Selective synthesis for light olefins from acetone over ZSM-5 zeolites with nano-and macro-crystal sizes, Appl. Catal., A, 403 (2011) 183-191.

[59] K. Na, C. Jo, J. Kim, K. Cho, J. Jung, Y. Seo, R.J. Messinger, B.F. Chmelka, R. Ryoo, Directing Zeolite Structures into Hierarchically Nanoporous Architectures, Sci., 333 (2011) 328-332.

[60] J. He, D. Chen, N. Li, Q. Xu, H. Li, J. He, J. Lu, Controlled fabrication of mesoporous ZSM-5 Zeolite-supported PdCu alloy nanoparticles for complete oxidation of toluene, Appl. Catal. B: Environ., 265 (2019) 118560. http://doi: 10.1016/j.apcatb.2019.118560.

[61] S. van Donk, A.H. Janssen, J.H. Bitter, K.P. de Jong, Generation, characterization, and impact of mesopores in zeolite catalysts, Catal. Rev., 45 (2003) 297-319.

[62] R. Chun, S. Kim, S. H. Han, A. K. Pandey, N. K. Mishra, I. S. Kim, Site-selective C−H nitration of *N*-aryl-7-azaindoles under palladium(II) catalysis, Tetrahedron Lett., 59 (2018) 3848-3852.

[63] S. Zhang, T. Shao, The impacts of aggregation and surface chemistry of carbon nanotubes on the adsorption of synthetic organic compounds, Environ. Sci. Technol., 43 (2009) 5719-5725.

[64] V. Sabna, S.G. Thampi, S. Chandrakaran, Adsorption of crystal violet onto functionalised multi-walled carbon nanotubes: Equilibrium and kinetic studies, Ecotoxicol. Environ. Saf., 134 (2016) 390–397.

[65] H. Anjum, K. Johari, N. Gnanasundaram, M. Ganesapillai, A. Arunagiri, I. Regupathi, M. Thanabalan, A review on adsorptive removal of oil pollutants (BTEX) from wastewater using carbon nanotubes, J. Mol. Liq., 277 (2019) 1005–1025.

[66] S. Mallakpour, S. Rashidimoghadam, 9 - Carbon Nanotubes for Dyes Removal, Composite Nanoadsorbents, Micro Nano Technol., Elsevier, (2019) 211-243. http://doi: 10.1016/B978-0-12-814132-8.00010-1.

[67] D.P. Dutta, R. Venugopalan, S. Chopade, Manipulating carbon nanotubes for efficient removal of both cationic and anionic dyes from wastewater, Chem. Select., 2 (2017) 3878–3888.

[68] N, Mozaffari. A, H, S, Mirzahosseini. A, H, Sari. L, F, Aval. Investigation of carbon monoxide gas adsorption on the Al_2O_3/$Pd(NO_3)_2$/zeolite composite film. Journal of Theoretical Appl. Phys., 14 (2019) 65–74.

[69] L. Samain, A. Jaworski, M. Edén, D. M. Ladd, D. K. Seo, F. J. Garcia-Garciad, U. Häussermanna, structural analysis of highly porous γ-Al2O3, J. Solid State Chem., 217 (2014)1–8.

[70] M. Shayesteh, M. S. Afarani, A. Samimi1, M. Khorram, Preparation of γ-Al_2O_3 and prioritization of affecting factors on the crystallite size using taguchi method, Trans. Phenom. Nano Micro Scales, 1 (2013) 45-52.

[71] J. Liu, j. Zhang, H. Zhang, F. Zhang, M. Zhu, N. Hu, X. Chen, H. Kita, Synthesis of hierarchical zeolite T nanocrystals with the assistance of zeolite seed solution, J. Solid State Chem., 285 (2020) 121228.

[72] N. M. Mahmoodi, M. H. Saffar-Dastgerdi, Zeolite nanoparticle as a superior adsorbent with high capacity: Synthesis, surface modification and pollutant adsorption ability from wastewater, Microchem. J., 145 (2019) 74-83.

[73] J.H. Kwak, J. Hu, D. Mei, C.W. Yi, D.H. Kim, C.H. Peden, L.F. Allard, J. Szanyi, Coordinatively unsaturated Al^{3+} centers as binding sites for active catalyst phases of platinum on gamma-Al_2O_3, Sci., 325 (2009) 1670-1673.

[74] S. Arnis, F. Belaib, M. Bencheikh Lehocine, H.-A Menian, Progress in clean energy, analysis and modeling,, Equilbrium and kinetic studies of adsorption of Cd(II), Zn(II), and Cu(II) from aqueous solution into cereal by-products, chapter 4, volume 1, Springer Publishing, (2015). https:// doi: 10.1007/978-3-319-16709-1

[75] D.M. Ruthven, principle of adsorption and desorption process, Wiley, New York, (1984).

[76] S.H. Chien, W.R. Clayton, Application of elovich equation to the kinetics of phosphate release and sorption in soils, Soli Sci. Soc. Am. j., 44 (1980) 265-268.

[77] A.O. Dada, D. F. Latona, O. J. Ojediran, O. O. Nath, Adsorption of Cu (II) onto bamboo supported manganese (BS-Mn) nanocomposite: effect of operational parameters, kinetic, isotherms, and thermodynamic studies, J. Appl. Sci. Environ. Manage., 20 (2016) 409 –422.

[78] S. Karka, S. Kodukula, S. V. Nandury, U. Pal, Polyethylenimine-modified zeolite 13X for CO_2 capture: adsorption and kinetic studies, ACS Omega, 4(2019) 16441 – 16449.

[79] A.A. Inyinbor, F.A. Adekola, G.A. Olatunji, Kinetics, isotherms and thermodynamic modeling of liquid phase adsorption of Rhodamine B dye onto Raphia hookerie fruit epicarp, Water Res. Ind., 15 (2016) 14–27.

[80] Y.S. Ho, G. McKay, Application of kinetic models to the sorption of copper (II) on to peat, Adsorp. Sci. Technol., 20 (2002) 797-815.